Inversions of Glacier Temperature Cross-Section Using Simulated Bistatic Radar Data and ADMM

Nicole Bienert
Department of Electrical Engineering
Stanford University
bienert@stanford.edu

Abstract

Traditional radar techniques measure depth averaged ice temperature and are unable to answer emerging questions about thermal influence on ice dynamics and the consequential impact on sea level rise. Here we present a new tool for testing ice temperature hypotheses by demonstrating in simulation that bistatic radar measurements paired with Alternating Direction Method of Multipliers (ADMM) processing enables inversion of the temperature distribution inside a glacier. The technique can discriminate between water channels, thermal anomalies, and a temperature gradient to asses which phenomena are influencing a particular ice stream. However, the resolution of this approach is limited, because the the transmitter and receiver must be on the surface of the glacier causing the inversion to be poorly constrained.

1. Introduction

Most of Antarctica's contribution to sea level rise originates from outlet glaciers and ice streams, which are fast moving pieces of ice surrounded by stagnant ice (see fig:1). The physical processes controlling ice stream width are poorly understood when topographic controls are absent, causing significant uncertainty in sea level rise predictions. Recent modeling studies indicate that ice stream width may be controlled by elevated temperatures along the ice stream's edge, an area called a shear margin [11]. At the edge of an ice stream, fast flowing ice is shearing against slow moving ice which creates heat and warms the ice in a distribution such as the one shown in figure 1. The warm ice is weaker its surroundings so it is hypothesized to cause shear localization, stabilizing the ice stream width. The attenuation of radar echos in ice is temperature-dependent due to the higher conductivity of warmer ice, suggesting that radar surveys should be able to test hypotheses relating ice stream geometry to internal temperature structure [5]. However, existing radars are predominantly monostatic and can only measure depth averaged attenuation which is insufficient for testing these hypotheses. Here, we demonstrate through simulation that bistatic measurements paired with an ADMM inversion has the potential to measure depth dependent temperature distributions at the spatial and thermal scale that can influence ice sheet flow and stability.

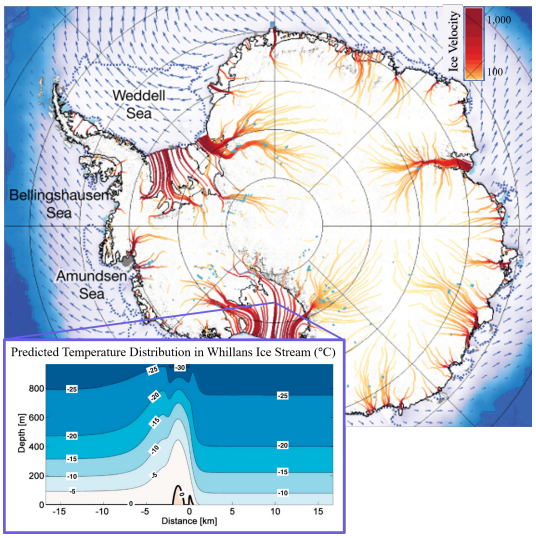

Figure 1. Ice speed in Antarctica as measured by satellite and a predicted shear margin temperature distribution. There is very little surface motion of interior ice and most of the motion is concentrated in ice streams and outlet glaciers. Figures from: [10, 11]

2. Related Work

Nearly all radars used in glaciology are monostatic. Since the transmitter and receiver are co-located these systems do not have sufficient independent measurements to accurately measure depth dependent temperature. Emerging monostatic data processing techniques utilize depth averaged attenuation, layer information, and thermodynam-

ics to model possible temperature depth profiles [9]. These methods require significant assumptions and cannot infer sufficiently small temperature differences for this application. Furthermore, this work is intended to test the theories predicting temperature anomalies, so it cannot make use of ice thermal physics in the measurements.

Bistatic systems vary the spatial separation between the antennas to generate quasi-independent measurements which could enable depth dependent temperature estimations. A few bistatic radar experiments have successfully used changing radio wave speed in uncompacted snow to estimate the density using inversion methods such as Gauss-Newton [2]. However, the snow on an ice sheet becomes compacted into ice and no longer has density fluctuations below 80-120m depth [2]. Density is the primary influence on ice permittivity and consequentially wave velocity. Temperature has a small influence on permittivity, causing it to change by 0.01 for a 25°C difference [7], but this causes too small of a time delay for small temperature gradients to be accurately measured by a bistatic system (which inherently has synchronization issues).

Instead of analyzing time of flight changes, received power can be used as a proxy for temperature. Temperature influences conductivity through the Arrhenius equation which influences attenuation and consequentially power received. Bistatic radar with offsets up to 2km has been implemented by [14] to accurately isolate conductivity from other influences on the received power by normalizing to the first measurement. They use a linear fit to solve for conductivity, but it can be isolated directly with the equation below where H is the ice thickness, variables with a 1 subscript are the first measurement and a subscript k indicates subsequent measurements.

$$\sigma = 2\sqrt{\frac{\epsilon}{\mu}}\frac{\ln\left(\frac{P_{RX\ K}G(\theta_1)\cos^2(\theta_1)\Gamma(\theta_1)^2}{P_{RX\ 1}G(\theta_k)\cos^2(\theta_k)\Gamma(\theta_k)^2}\right)}{-2H\left(\frac{1}{\cos(\theta_k)}-\frac{1}{\cos(\theta_1)}\right)} \tag{1}$$

This idea was taken a step farther by [4], where the authors used englacial layer reflectors and the equation above to measure depth averaged ice conductivity to a particular depth of reflector. However, the results suffered from poor signal to noise ratio of the internal reflectors. Therefore, we introduce ADMM inversions to solve depth dependent conductivity using only the high SNR basal reflection.

3. Background Theory

3.1. Received Power

The power received by the radar is influenced by several factors including the transmitted power (P_{TX}), wavelength (λ), and distance the wave traveled (r). Many variables have angular dependence including the antenna gains (G), scattering (ρ), and the reflection coefficient (Γ). The bedrock or till under the glacier is a planar, mirror-like reflector which causes the power to continue spreading at $1/r^2$ rather then having the $1/r^4$ characteristic of a point scatterer.

$$P_{RX} = P_{TX}G_1G_2\rho\left(\frac{\lambda}{4\pi r}\right)^2\Gamma^2 e^{-2\alpha r} \tag{2}$$

The attenuation coefficient (α) is simplified to the following equation because ice is a low loss medium ($\frac{\sigma}{\omega\epsilon_r\epsilon_0} \approx 1x10^{-3} << 1$) [12]. Warmer ice is more conductive which increases the attenuation experienced by an electromagnetic wave and decreases the received power.

$$\alpha = \frac{\sigma}{2}\sqrt{\frac{\mu}{\epsilon}} \tag{3}$$

3.2. Arhenius Equations

The relationship between conductivity and temperature is not straightforward because an ice sheet is not pure water. The composition of precipitation has fluctuated over the past 800,000 years and includes layering from volcanic eruptions and acidic precipitation [3]. These materials have different conductiviteis and consequentially, different values in the arhenius equations. Matsuoka and MacGregor modeled the relation between temperature and conductivity which is given below in equation 4 [6] [5]. The equation accounts for the conductivity contributions of pure ice (i=0), H+ ions (i=1), and salt (i=2). The equation excludes other contributing compounds, such as NH4+ which may play a dominant role in Greenland, but not Antarctica.

$$\sigma = \sum_{i=0}^{2}\sigma_i^0 C_i e^{-\frac{E_i}{k}(\frac{1}{T}-\frac{1}{T_r})} \tag{4}$$

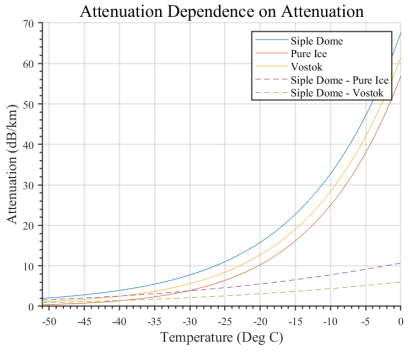

Figure 2. Attenuation vs temperature for different ice chemistries.

The molar conductivity of each material is σ^0, C is the concentration of each compound, E is the activation energy, k is boltzman's constant, T is the temperature in kelvin, and T_r is the reference temperature at which the measurements were made. The attenuation as a function of temperature

and ice composition is plotted in figure 2. The attenuation was calculated from conductivity as atten = $0.914\text{x}10^6\sigma$ dB/km.

It can be seen in figure 2 that the locations Siple Dome and Vostok have different attenuations up to about 6dB/km. While ice chemistry evidently alters the attenuation, it is a smaller influence than temperature. This paper will use the Siple Dome concentrations measured by MacGregor in simulations, but applications of this technique should use measurements from the nearest ice core.

4. Methods

4.1. Overview

Bistatic measurements will be taken in a common shot gather formation where the transmitter is stationary and the receiver is moved in increments between measurements. This geometry is preferred because it requires only a two person team (two for safety). As the receiver moves away from the transmitter, the received power decays according to the power equation (eq:2). The rate of decay is related to the electrical properties of the ice through the attenuation coefficient (eq:3). The permittivity can be treated as constant and the material is non-magnetic, so $\mu = \mu_0$. However, the conductivity fluctuates significantly with temperature (eq:4). The cross section of the ice sheet can be gridded up into blocks of different conductivities (see fig:3) which can be estimated with inverse theory, then the temperature can be solved for from conductivity using gradient descent.

4.2. ADMM Inversion for Conductivity

All parameters in the power equation are known except for the reflection coefficient and conductivity. As an initial demonstration, we will assume that the reflection coefficient is also known. Ray theory can be used to write the received power in terms of the electrical properties of each grid space and the distance (Δr_n) the ray travels through each grid space. The power at receiver k is given by:

$$P_k = P_{TX} G^2(\theta_k)\, \rho\Gamma_k^2(\theta_k) \left(\frac{\lambda}{4\pi r_k}\right)^2 e^{-\sum_{n=1}^{Ngrids} \frac{\sigma_n}{2}\sqrt{\frac{\mu}{\epsilon}}\Delta r_{k,n}}$$

The only variables dependent on the grid number (n) are the conductivity and distance the ray travels through that grid (Δr_n). We can rewrite the equation above to separate the variables dependent on the grid number:

$$\sum_{n=1}^{Ngrids} \sigma_n \Delta r_{k,n} = \frac{-2\ln(P_k)}{\sqrt{\frac{\mu}{\epsilon}}\ln\left(P_{TX} G^2(\theta_k)\, \rho\Gamma_k^2(\theta_k)\left(\frac{\lambda}{4\pi r_k}\right)^2\right)}$$

This is now in the $Cx = b$ format where b is the right hand side of the equation, which is the measured power normalized by the other parameters in the power equation. The

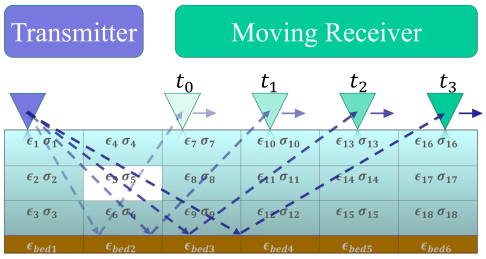

Figure 3. Conceptual depiction of electrical property inversions enabled by this work, where a common shot gather will be used for safety. An inversion constrains the properties of each grid using the rays that pass through it; for example, the white grid's properties would be constrained by the depicted rays.

conductivity matrix is x, while C is the Δr mask that selects which conductivity grid a ray passed through and weights that grid by the length of the ray in that grid. We want to find conductivities that minimize $Cx - b$ and make the forward model match the normalized power data (b). That minimization problem is underdetermined, because there are more conductivity grids than power measurements, and the constraint that the transmitter and receiver need to be on the surface of the ice prevents measurements from being completely independent.

There are an infinite number of conductivity distributions that would match the data, so we introduce a TV prior to limit the solutions to this problem. The TV prior promotes piecewise linear conductivity distributions. This is desirable, because it prefers smooth solutions, but doesn't smooth edges. This is ideal, because most conductivity structures we anticipate in the ice are smooth temperature transitions, but some structures cause abrupt conductivity changes including subglacial channels and aquifers. It is important that the method can detect subglacial channels, because past studies have found liquid water in the shear margin and extrapolated that this influences the width of the ice stream [8]. The TV prior is added to the $Cx - b$ minimization problem below:

$$\text{Minimize}\frac{1}{2}\left|\left|\begin{bmatrix}\Delta r_{1,1} & \cdots & \Delta r_{1,n}\\ \vdots & \ddots & \vdots \\ \Delta r_{k,1} & \cdots & \Delta r_{k,n}\end{bmatrix} - \begin{bmatrix}b_1\\ b_2\\ b_3\end{bmatrix}\right|\right|_2^2$$
$$-\lambda\left|\left|\begin{bmatrix}\nabla_x\\ \nabla_y\end{bmatrix}\begin{bmatrix}\sigma_1 & \cdots & \sigma_{rows}\\ \sigma_2 & \ddots & \vdots \\ \sigma_3 & & \\ \sigma_{cols} & \cdots & \sigma_n\end{bmatrix}\right|\right|_1$$

The L1 norm is non-differentiable, so the problem is re-

written as a constraint problem that can be solved.

$$\min \frac{1}{2}||Cx - b||_2^2 + \lambda|z|_1$$
$$\text{Constraint: } z = \begin{bmatrix} \nabla_x \\ \nabla_y \end{bmatrix} x$$

This can be solved with an augmented Lagrangian that penalizes solutions nearing the constraint boundary.

$$L_\rho(x, y, z) = \frac{1}{2}||Cx - b||_2^2 + \lambda|z|_1$$
$$+y^T(\begin{bmatrix} \nabla_x \\ \nabla_y \end{bmatrix} x - z) + \frac{\rho}{2}||\begin{bmatrix} \nabla_x \\ \nabla_y \end{bmatrix} x - z)||_2^2$$

The ADMM algorithm presented on page 43 of [1] and reviewed in [13] is then applied to minimize this problem. ADMM splits the problem into two minimizations tied by a scaled dual variable ($u = \frac{1}{\rho}y$) which promotes steps towards maintaining the constraint. The Lagrangian is first minimized with respect to x, sequentially minimized with respect to z, and then u is updated. The code loops over the following updates:

X Update: Solve for x using matlab's pcg function

$$v = z - u$$
$$C^T b + \rho\nabla^T v = (C^T C + \rho\nabla^T\nabla)x$$

Z Update: Soft Threshold

$$v = \nabla x + u$$
$$z = \begin{cases} v - k & v > k \\ 0 & \text{otherwise} \\ v + k & v < -k \end{cases}$$

U Update:

$$u = u + \nabla x - z$$

4.3. Retrieve Temperature from Conductivity

After estimating the conductivity grid using ADMM, equation 4 can be used to invert for temperature. There isn't an analytical solution, but it can be solved numerically with gradient descent. The concentrations of pure ice, acids, and salt are linearly interpolated to the grid center from the Siple Dome data in [5] (see fig:4). These are used in the forward model to compute the conductivity for each temperature update. The temperature update is incremented by the residual times a parameter controlling the step size (d).

loop

$$\text{step} = d(\sigma_{\text{measured}} - \sigma(T))$$
$$T = T + \text{step}$$

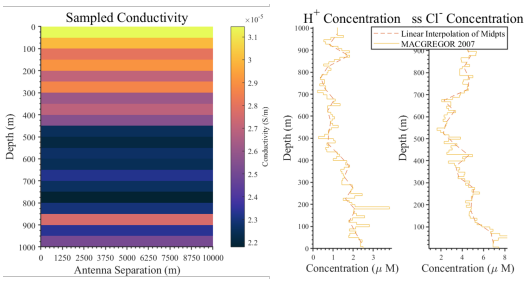

Figure 4. Conductivity grid forward modeled for -15°C from the salt and acid concentration interpolated from [5].

5. Results

Inversions were conducted with 60 measurements on a 20x40 grid spanning a 1,000m x 10,000m piece of ice. This geometry was chosen, because temperate zones in shear margins are expected to be a few kilometers wide, so a 10km transect would capture the distribution. A 1km ice depth was used, because it is within the typical ice thicknesses range and the conductivity data from MacGregor only extends to 1km. Three temperature distributions were simulated for each inversion. The temperature hypothesis we aim to test predicts roughly a Gaussian distribution caused by shear heating [11]. Subglacial channels may exist under shear margins, so a subglacial channel was simulated as a temperate ice circle hovering just below 0°C. Normal ice was simulated as a linear temperature gradient from -26°C at the surface to 0°C at the bed.

The ADMM inversion was simulated for different ray geometries and can be compared against a traditional technique, the Winebrenner CMP which uses equation 1 to compute average conductivity. The results are shown in figure 6. The final PSNR is displayed above each image. The ADMM inversions are poorly conditioned because the transmitter and receiver must be on the surface of the glacier, and this causes instability in the inversion (see fig:**??**. The single transect ADMM inversions were only run for 50 iterations, because the solution would blow up after that. Stability improved with more transects.

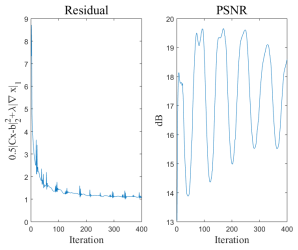

Figure 5. Residual and PSNR for the Gaussian temperature distribution inversion with three transects. This is the most unstable inversion when three transects were used.

6. Discussion

The ADMM inversion using three asymmetric transects distinctly reconstructs the three modeled temperature distributions with PSNR values of 18.6dB, 12.3dB, and 29.7dB. For the temperature gradient, it correctly determines that the surface is cooler than the bed, but it has an error in the bottom right corner where there is only monostatic data. The gaussian temperature is roughly inverted to be a warm blob at the bottom middle of the inversion space. The subglacial channel is very accurately inverted with the exact channel size being recovered. All the temperature distributions have horizontal stripes which are caused from the inversion smoothing the conductivity solution. When the smooth conductivity solution is mapped to temperature accounting for the changing layer composition (see fig:4), the layering is mapped into temperature.

ADMM inversions with at least two transects perform better than the Winebrenner CMP which only computes the average temperature. The Winebrenner CMP has a better PSNR for some of the temperature distributions, but averages out any features in the ice and fails to meet the goal of measuring a temperature distribution. One transect does not provide sufficient independent measurements to invert the conductivity accurately and causes features to be blurred out. Two symmetric transects, one with the receiver moving from left to right (0km to 10km) and the other moving from 10km to 0km, provides improved resolution and correctly inverts for the subglacial channel. Both the temperature gradient and Gaussian temperature distribution display diagonal smearing caused by the redundant measurements when the transmitter and receiver are at 0km and 10km. Asymmetric measurements prevent redundancies and introduce more independent data for a better inversion. Resolution improves with more asymmetric transects.

7. Conclusion

ADMM enables differentiating between different temperature structures; however, it does not provide the resolution necessary for a quantitative comparison with thermal predictions with only three transects. More transects provide better spatial resolution, but become physically intractable in a field season where time is finite. Regardless, the ADMM inversion enables scientists to determine if a hypothesized phenomenon exists, which is not possible with current techniques that only measure depth averaged temperature. Our technique leverages quasi-independent measurements provided by bistatic radar with asymmetric transects. ADMM is used to invert for the conductivity distribution, then gradient descent isolates depth dependent temperature from the Arrhenius equations. This method accurately reconstructed the three temperature distributions modeled: a linear temperature gradient, a Gaussian distribution, and a subglacial channel. Further work is required to add the reflection coefficient into the inversion. The method we introduce demonstrates the plausibility of thermal tomography and is an important step towards estimates of temperature distributions at the spatial and thermal scale that can influence ice sheet flow and stability.

References

[1] S. Boyd, N. Parikh, E. Chu, B. Peleato, J. Eckstein, et al. Distributed optimization and statistical learning via the alternating direction method of multipliers. *Foundations and Trends® in Machine learning*, 3(1):1–122, 2011.

[2] R. Drews, J. Brown, K. Matsuoka, E. Witrant, M. Philippe, B. Hubbard, and F. Pattyn. Constraining variable density of ice shelves using wide-angle radar measurements. *Cryosphere*, 10(2):811–823, 2016.

[3] N. S. F. I. C. Facility. About ice cores. Available at `https://icecores.org/about-ice-cores` [3/12/2020].

[4] N. Holschuh, K. Christianson, S. Anandakrishnan, R. B. Alley, and R. W. Jacobel. Constraining attenuation uncertainty in common midpoint radar surveys of ice sheets. *Journal of Geophysical Research: Earth Surface*, 121(10):1876–1890, 2016.

[5] J. A. MacGregor et al. Modeling englacial radar attenuation at siple dome, west antarctica, using ice chemistry and temperature data. *J. Geophys. Res. Earth Surf.*, 112(F3), 2007.

[6] K. Matsuoka, J. A. MacGregor, and F. Pattyn. Predicting radar attenuation within the antarctic ice sheet. *Earth and Planetary Science Letters*, 359:173–183, 2012.

[7] T. Matsuoka, S. Fujita, and S. Mae. Effect of temperature on dielectric properties of ice in the range 5–39 ghz. *Journal of Applied Physics*, 80(10):5884–5890, 1996.

[8] J. D. Platt, T. Perol, J. Suckale, and J. R. Rice. Determining conditions that allow a shear margin to coincide with a röthlisberger channel. *Journal of Geophysical Research: Earth Surface*, 121(7):1273–1294, 2016.

[9] D. M. Schroeder, H. Seroussi, W. Chu, and D. A. Young. Adaptively constraining radar attenuation and temperature across the thwaites glacier catchment using bed echoes. *J. Glaciol.*, 62(236):1075–1082, 2016.

[10] A. Shepherd, H. A. Fricker, and S. L. Farrell. Trends and connections across the antarctic cryosphere. *Nature*, 558(7709):223–232, 2018.

[11] J. Suckale et al. Deformation-induced melting in the margins of the west antarctic ice streams. *J. Geophys. Res. Earth Surf.*, 119(5):1004–1025, 2014.

[12] F. Ulaby and R. Umberto. *Fundamentals of Applied Electromagnetics*. Pearson, Upper Saddle River, New Jersey 07458, 7 edition, 2015.

[13] G. Wetzstein. Ee367 lecture 11: Compressive imaging. Available at `http://stanford.edu/class/ee367/` [2/28/2020], 2020.

[14] D. P. Winebrenner, B. E. Smith, G. A. Catania, H. B. Conway, and C. F. Raymond. Radio-frequency attenuation beneath siple dome, west antarctica, from wide-angle and profiling radar observations. *Annals of Glaciology*, 37:226–232, 2003.

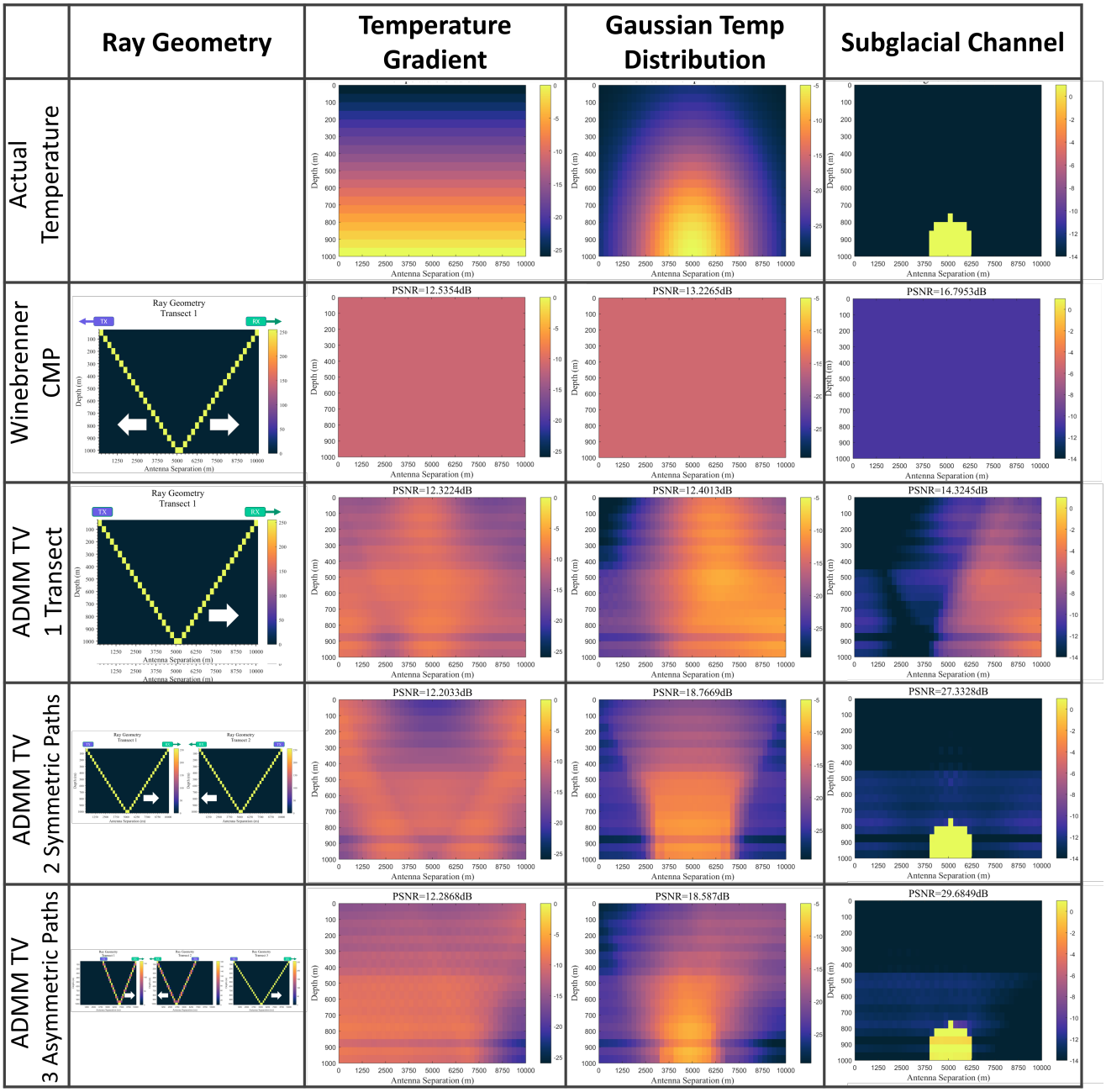

Figure 6. Comparison of ADMM technique against the traditional Winebrenner Common Mid-Point (CMP) measurement for inverting a temperature distribution (in degrees Celcius). The actual temperature distributions are depicted in the top row and include a gaussian temperature distribution, which is expected in shear margins, a warm subglacial channel, and a plain temperature gradient for the lack of a thermal anomaly. Traditional techniques like the Winebrenner CMP technique only measure depth averaged temperature. Application of ADMM enables resolving features in the ice. All of the inversions use 60 measurements, but the ADMM techniques with more asymetric transects perform better since the measurements are closer to independent. The extent of each transect is depicted in the first column where the white arrow indicates the motion of the receiver. For the ADMM inversion, the transmitter is stationary, but the CMP takes measurements with both the transmitter and receiver moving away from each other in equal increments.